Quantification of macromolecular crowding and ionic strength in living cells

Liu, Boqun

Chapter 4

Macromolecular crowding during adaptation to hyperosmotic stress

Manuscript in preparation

Abstract

Cellular macromolecular crowding influences the mobility of biomolecules, protein folding and stability, and the association of macromolecules with each other. To understand how macromolecular crowding changes during adaptation to hyperosmotic stress, we tracked the crowding changes in *Escherichia coli* with previously developed macromolecular crowding sensors (crGE, crE6, and crG18). The results demonstrate that macromolecular crowding increases immediately after osmotic upshift, then decreases to a lower level over 2-5 h, where it remains for several hours. The crowding initially follows cell volume but arrives at a lower value upon adaptation. With these results, in combination with literature observations, we hypothesize that the decrease could be due to an increase in self-association of the macromolecules in the cell upon adaptation. The self-association creates a heterogeneous distribution in the cytoplasm, resulting in some regions experiencing less crowding. This interpretation would be fundamental to the organization of the crowded cellular cytoplasm, and could apply to other species as well.

Introduction

The cellular environment is highly crowded with proteins and other macromolecules[1]. Many biochemical and biophysical processes, such as gene expression[2], macromolecule diffusion[3], protein-DNA interaction[4,5], and protein folding[6,7] are affected by macromolecular crowding. However, the cellular environment is not static and the volume of a cell undergoes changes when unicellular organisms are confronted with changes in the osmolality of the extracellular environment. These changes have consequences for physicochemical parameters such as crowding, ionic strength, pH, viscosity and osmotic pressure.

Cells will adjust their cytoplasm to counteract the consequences of the osmotic stress. Upon osmotic upshift, the cells immediately shrink[8] and many cells counteract this by taking up potassium ions, which is best documented for *E. coli9*. Subsequently, *E. coli* synthesizes or takes up available compatible solutes[10,11], and adjusts the proteome to adapt to the osmotic upshift. Researchers[12–16] showed that in *E. coli* over 300 genes are up- or downregulated by osmotic upshift. Interestingly, Konopka et al.[17] found that the biopolymer fraction increases after adaptation to hyperosmotic shock, while the diffusion coefficient of GFP only shows a small decrease. These findings indicate that there may be significant changes in the molecular crowding and biopolymer organization in the cytoplasm during adaptation of *E. coli*.

Previously, we developed a set of FRET-based crowding sensors[18,19]. The sensors allow one to track temporally the macromolecular crowding during osmotic stress. In this chapter, we employ three sensors, which have different linker structure and sensing properties *in vivo*. The crGE is the largest crowding sensor, which consists of two α-helices three random coils, with fluorescent proteins (donor and acceptor) connected to the N- and C-terminal ends. The crE6G2 sensor consist of two α-helices one small random coil and the fluorescent proteins. The crG18 sensor consist of a single long random coil and is least sensitive to crowding changes in *vivo* (chapter 2). We show that macromolecular crowding increases upon osmotic upshift and returns within 2-5 hours to a level lower than the crowding prior the osmotic shift. We explain the lower apparent crowding with the hypothesis that the macromolecules in adapted cells increasingly associate with each other (perhaps forming areas where the sensor is excluded), which creates regions of lower crowding.

Material and Methods

Cell growth and confocal imaging

The batch culture experiments were performed as described previously[18,19]. The *E. coli* cells with the appropriate plasmids were prepared as described in Chapter 2. Briefly, the pRSET A vector containing the synthetic gene encoding either crGE, crE6G2 or crG18, was transformed into *E. coli* BL21(DE3) pLysS. The cells were incubated at 30 °C, shaking at 200 rpm, in 10 mL MOPS medium[20] with 20 mM glucose and grown overnight. The next day, the cells were diluted into 50 mL of fresh medium to OD_{600} = 0.05. When the OD_{600} reached 0.1–0.2, the cells were exposed to the desired amount of NaCl and imaged under the microscope as described in Chapter 2. In short, 0.5 mL cells, expressing one of the sensors, were combined with 0.5 mL cells without sensor (blank). The combined cells were centrifuged, and resuspended in 100 µL (MOPS minimal medium with 20 mM glucose and the desired amount of NaCl (osmotic upshift). Subsequently, the cells were transferred to a glass slide [coated/treated coverslip modified with (3-aminopropyl) triethoxysilane] and imaged on a laser-scanning microscope (Zeiss LSM 710) immediately after the osmotic upshift.

Imaging in a microfluidics chamber

The microfluidic chamber (CellASIC ONIX Microfluidic Plates) was pre-warmed overnight at 30 °C on the laser-scanning confocal microscope. The *E. coli* BL21(DE3) pLysS strain with desired crowding sensor and the control strain were grown overnight to an OD_{600} of 0.1-0.3, which is still in the exponential growth phase, and they were then diluted to OD_{600} = 0.01 in MOPS minimal medium with 20 mM glucose and subsequently loaded in the microfluidic chamber. After loading, the cells were incubated with 0.1× MOPS-glucose medium (MOPS-glucose medium diluted ten times with 0.16 M NaCl) at 30 °C for 2 h. For the osmotic upshift, 0.3 M NaCl in the 0.1× MOPS-glucose medium was flowed in 2h after the cells were loaded, to allow the cells to adapt to the new environment. Alternatively, we used 600 mM and 1 M sorbitol in 0.1x MOPS-glucose for osmotic upshift in the microfluidic chamber. The images were collected and analyzed as described previously[18,19].

Cell volume determination

The volume of the cytoplasm was determined by PhotoActivated Localization Microscopy (PALM). The gene encoding LacY was fused to YPet which can switch "on" or "off" during imaging in PALM[21]. The gene encoding LacY-Ypet was cloned into pACYC and transfected into *E. coli* BL21(DE3) pLysS. The cells (inoculated from a single colony) were grown at 30 °C, shaking at 200 rpm in 10 mL MOPS medium with 20 mM glucose, overnight. The next day, when OD_{600} reached 0.2, the cells were induced with 0.1% rhamnose. One hour after induction, the cells were imaged by PALM microscopy before and after addition of 300 mM NaCl.

Coverslips were cleaned with 5M KOH in a sonication bath for 30 minutes, and washed with demineralized water and acetone (Aldrich). Next, the coverslips were plasma-cleaned for 10 min, and subsequently coated with 2% (v/v) (3-Aminopropyl) trioxysilane (Aldrich) in acetone for 30 minutes. The coverslips were washed with demineralized water and left drying.

For PALM, a home-built inverted microscope based on an Olympus IX-81 with a high numerical aperture objective (100 X, NA = 1.49, oil immersion, Olympus, UApo) was used. Solid-state lasers were from Coherent (Santa Clara, USA): 514nm (Sapphire 514, 100mW). Imaging was performed in semi-TIRF mode with the angle of light exiting the objective adjusted to create a light sheet restricted to the bottom few micrometers of the specimen. The fluorescence was recorded using an electron multiplying charge-coupled device (EM-CCD camera) from Hamamatsu, Japan, model C9100-13. For data acquisition and analysis, LacY-YPet was continuously illuminated at 517 nm and a total of 3000 frames were recorded with 30 ms for each frame. The data was analyzed with a home-written ImageJ script, in which the reconstructed images of each fluorescent molecule are represented as a single spot at its determined coordinates, with a brightness that corresponds to the localization accuracy [22].

Preparation of cell lysate

The *E. coli* BL21(DE3) pLysS cells were incubated in 10 mL MOPS with 20 mM glucose at 30 °C and shaking at 200 rpm overnight, and then diluted to 1 L of fresh medium to OD_{600} = 0.02. When the OD_{600} reached 0.2, half of the culture was lysed immediately, while the other half was lysed after incubation for 5 h with 300 mM NaCl. To lyse the cells, the cultures were harvested by centrifugation (3000× g, 30 minutes). The pellet was resuspended in phosphate buffer (10 mM NaPi, 100 mM NaCl, pH 7.4) containing proteinase inhibitor (cOmplete™,

Mini, EDTA-free). Cells were lysed by sonication for 2 minutes, with alternating 5 seconds sonication and 5 seconds cooling, and then centrifuged (20,000xg, 10 min). The supernatant was immediately used for the fluorescence measurements.

Fluorometry

Fluorescence emission spectra were measured with a Fluorolog-3 (Jobin Yvon) spectrofluorometer as described in Chapter 2. A 1.0 mL solution (10 mM NaPi, 100 mM NaCl, 2 mg/mL BSA, pH 7.4) was added to a quartz cuvette and its fluorescence emission spectrum was recorded after excitation at 420 nm (A). Subsequently, purified sensor was added, mixed by pipette, and the fluorescence was recorded (B). The desired amount of small molecule or cell lysate was added, mixed by pipette, and the fluorescence was recorded again (C). The background spectrum A, prior to the addition of the probe, was subtracted from B or C.

The influence of small molecules on the read-out of the crowding sensor (crG18) was recorded on a Spark® 10M microplate reader. A 300 µL solution containing the given small molecule (Proline, KCl, ATP, sucrose and aspartic acid) and 10 mM NaPi (adjusted the pH to 7.4 after dissolution of the salts) were added to a 96 well plate (Greiner). The purified sensor was added and the fluorescence intensity at 475 nm and 525 nm were recorded separately with excitation at 420 nm at room temperature. A 20 nm bandwidth for excitation and emission was applied, and the average of 10 measurements of a single well was taken. The background fluorescence (buffer without sensor) was subtracted in all cases.

Results

Temporal changes in apparent crowding upon osmotic upshift

Cells in batch culture

To track the changes in crowding during adaptation to hyperosmotic stress, we grew *E. coli* BL21(DE3) pLysS containing the crGE sensor in a 50 mL MOPS-glucose medium, and exposed the cells to an osmotic stress of 300 mM NaCl when the OD_{600} reached 0.2. We diluted the culture throughout the experiment to maintain the OD_{600} between 0.1 and 0.3, and corrected the OD_{600} for dilution (Fig. 1). We took samples for imaging from the culture to monitor the temporal change of ratiometric FRET of crGE (Fig 1A). The FRET value is 1.06 ± 0.009

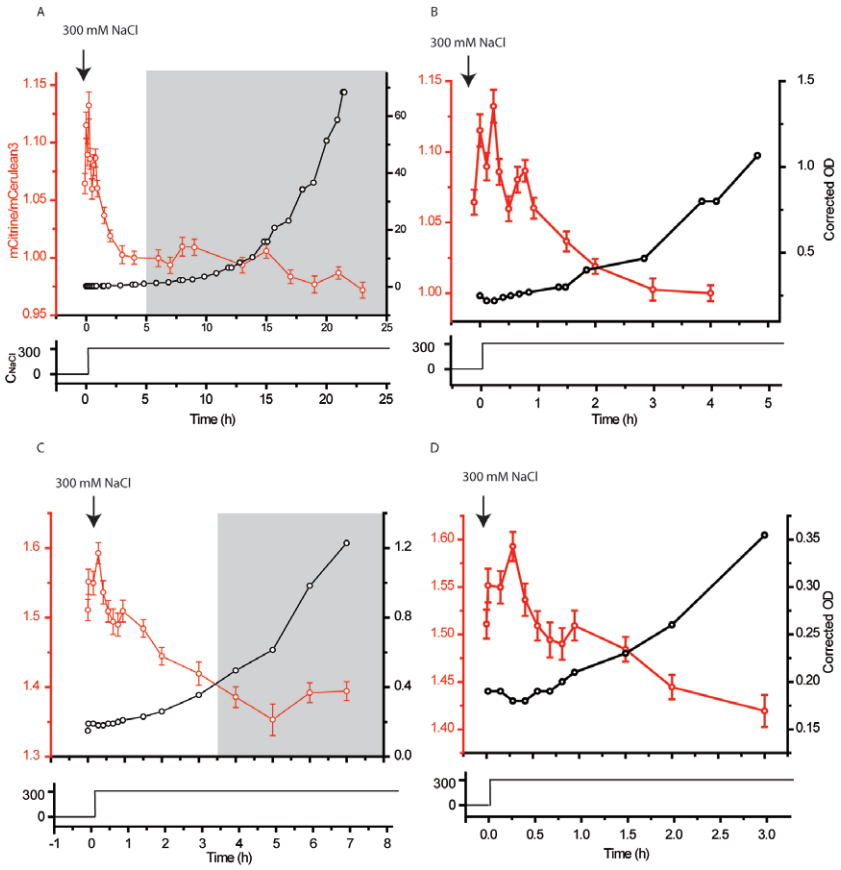

Fig. 1. Crowding changes upon osmotic upshift in cells in batch culture. *The concentration of NaCl is shown in the upper lane of each graph, and the grey shaded area indicates when the crowding remains at a lower level.* ***A:*** *The ratiometric FRET of crGE in E. coli growing in 50 mL culture at 30 °C. The cells were shocked with 300 mM NaCl. We diluted the culture throughout the experiment to maintain the OD600 between 0.1 and 0.3; the corrected OD reflects OD600 times the dilution factor. The point before t = 0 indicates before NaCl addition. Error bars are the standard error (n = ~100 cells).* ***B:*** *The zoom-in of panel A.* ***C:*** *The same as A, except that crG18 was used.* ***D:*** *The zoom-in of C.*

(s.e., n = 98) before the upshift, and immediately increases to 1.12 ± 0.01 (s.e., n = 98) upon addition of NaCl. The ratiometric FRET returns to the level before the osmotic upshift within 1 h and decreases to 1.00 ± 0.006 (s.e., n = 90) over the next 3 h. The ratiometric FRET remains at the lower level for at least 23 h. We observed a similar decrease when the crowding was probed by the crG18 sensor under the same conditions (Fig. 1B). Hence, the observations are independent of the structural properties of the crowding sensor. We found in

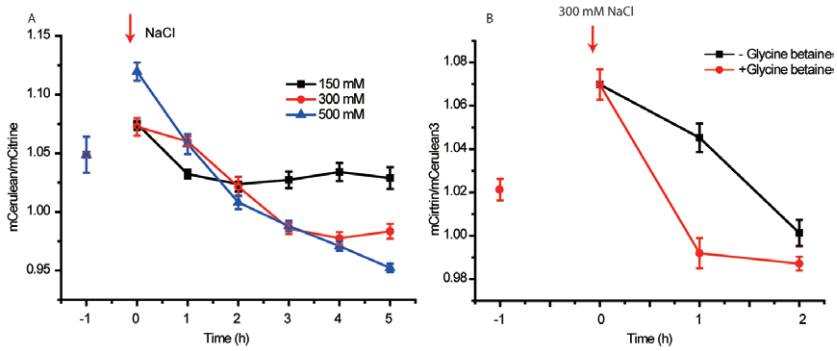

***Fig. 2. Adaptation to osmotic stress at different degrees of upshift. A**: E. coli BL21(DE3) pLysS with crGE sensor was incubated in MOPS-glucose at 30 °C in batch culture. Just before t = 0, the cells were treated with different concentrations of NaCl. **B:** The same as panel A, except that 1 mM glycine betaine was present in the medium. Errors bars show the standard error over ~100 cells.*

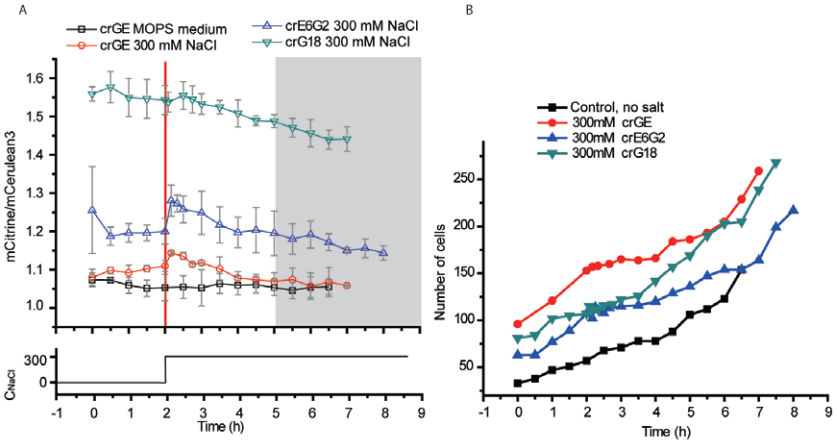

***Fig. 3. Crowding changes upon osmotic upshift in cells in the microfluidic chamber. A**: Ratiometric FRET of different sensors in the microfluidic chamber. Cells were grown in the chamber in 10-times diluted MOPS-glucose plus 0.16 M NaCl, which has a similar osmolality as MOPS-glucose. At 2 h, the same medium supplemented with 300 mM NaCl was flowed in. The black squares show the data of cells that were not subjected to an osmotic upshift. Error bars show the standard deviation from three independent biological replicates, each based on ~100 cells. **B**: The cell number of E. coli growing in the microfluidic chamber.*

both cases that the cell stopped growing from 0 to 1h during which the crowding returned to the level before shock. After 1h, the OD_{600} resumed but the crowding decreased further.

To compare the influence of osmolality on the apparent decrease in crowding in the adaptation period, we treated the cells with

different concentrations of NaCl (Fig. 2A). We found that the final ratiometric FRET after adaptation decreases with increasing osmolality (Fig. 2A). This indicates that the overshoot of crowding is not a switch between two distinct states of the cytoplasm but occurs on a continuous scale.

To investigate the influence of compatible solutes on the recovery of the cells, we treated the cells with 300 mM NaCl in the presence of glycine betaine (Fig. 2B). Compatible solutes, such as glycine betaine, aid the cell in surviving osmotic upshifts by balancing the osmotic difference and stabilizing the proteins[23]. The compatible solutes only slightly decrease the ratiometric FRET by increasing the refractive index of the medium, as described previously[18]. We observed that the ratiometric FRET levels off to the same value in the presence and absence of glycine betaine, but the restoration of crowding is faster in the presence of glycine betaine[24]. The cells were not primed with glycine betaine, which would induce the expression of the corresponding transporters (ProP, ProU; add REFS), yet the recovery is still faster than without glycine betaine.

Cells in microfluidic chamber

To obtain further information on the transients in the crowding, we tracked individual cells in a microfluidic chamber (Fig 1C). We first determined the ratiometric FRET of *E. coli* growing in 0.1× MOPS-glucose medium (supplemented with 160 mM NaCl). The crowding stays stable during the 6 h period, confirming unperturbed growth (Fig. 3A). We observed smaller changes in apparent crowding when cells grew in 0.1× MOPS-glucose medium compared to undiluted MOPS-glucose medium, for which for which we currently do not have an explanation. Additionally, we found that the growth rate in 0.1× MOPS-glucose medium and MOPS-glucose medium are similar, which is ~0.5 h^{-1}. Hence, for all the experiments in the microfluidic chamber, we incubated the cells in 0.1x MOPS-glucose medium, supplemented with 160 mM NaCl.

For experiments where cells were challenged with osmotic stress, the cells were first incubated in the microfluidic chamber for 2 h, after which we continuously flowed in medium with 300 mM NaCl. To confirm that crowding changes were independent of the type of crowding sensor, we compared the FRET signals of crGE, crE6G2 and crG18 during the osmotic upshift. We find a similar decrease in ratiometric FRET as observed in the experiments in batch culture. The number of cells was counted (Fig 3B). During the first 2h before upshift, the cell number increased steadily indicating the cells grow well in the microfluidic device. The cell number stopped to increase when the medium when 300 mM NaCl was flowed in. The cells started to grow again at ~4 h.

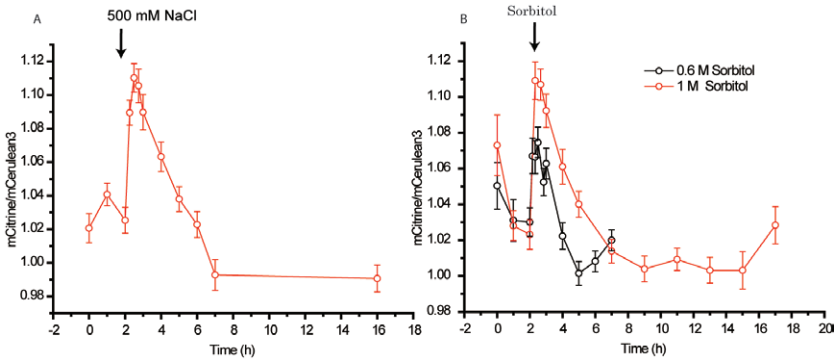

Fig. 4. Crowding changes in cells in the microfluidic chamber upon osmotic upshift with NaCl or sorbitol. A: *The E. coli BL21(DE3) pLysS cells expressing crGE were loaded into a microfluidic chamber at t = 0 and incubated at 30 °C in 0.1x MOPS-glucose medium. At t = 2h, 0.1x MOPS-glucose with 500 mM NaCl were flowed in. Errors bars are standard error over ~100 cells.* ***B:*** *The E. coli BL21(DE3) pLysS cells expressing crGE sensors were treated the same as A. At = 2h, 0.1x MOPS-glucose medium with desired concentration sorbitol were flowed in. Errors bars show the standard error in the FRET ratio from ~100 cells.*

For crGE and crE6G2, the ratiometric FRET increases instantaneously by flowing in NaCl and then decreases to a level lower than before the osmotic upshift. The lower level is reached after ~4h when the cells also resume growth. The crG18 sensor, which is less sensitive than crGE and crE6, shows accordingly a much smaller increase in ratiometric FRET (Fig. 1B). Similar to the measurements for cells growing in batch culture, the apparent crowding levels off to a lower value with 500 than 300 mM NaCl. To confirm that the decrease is independent of the nature of the osmolyte to stress the cells, we also performed osmotic perturbations with sorbitol in the microfluidic chamber (Fig. 4), and made similar observations as for NaCl.

Volume and length of cells exposed to osmotic stress

To investigate the relation between the apparent crowding changes and cell volume, the volume of the *E. coli* cytoplasm was determined from images obtained by PALM, using the membrane protein LacY fused to the yellow fluorescent protein Ypet to mark the cytoplasmic compartment. The volume decreases by 30% after adding 300 mM NaCl (**Fig. 5A**). Three hours after the osmotic upshift, the volume has recovered to ~1.8 fL, which is 82% of the value before the shock. Next, to yield more detail of the structural changes of the cell, we determined the length (**Fig. 5B, C**) of the cells grown in batch culture (Fig. 1B, C). The cells immediately become shorter by 20% upon addition of

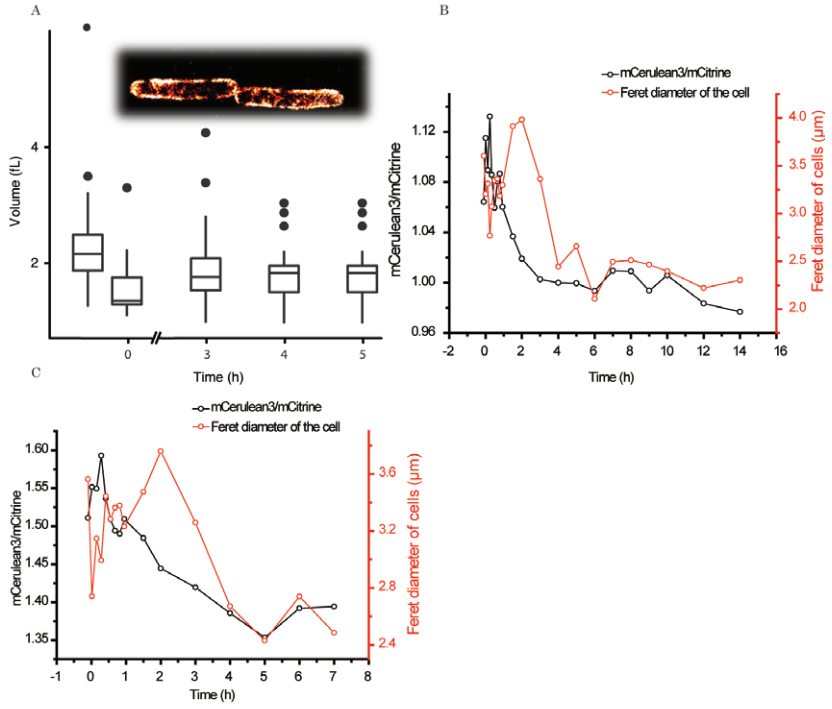

Fig. 5. Cell volume and length during hyperosmotic stress. A: *Volume of E. coli BL21(DE3) pLysS expressing LacY-YPet, and determination of the cell contours from single-molecule localizations by PALM microscopy. At t = 0, the cells were treated with 300 mM NaCl. For each data point, ~30 cells were imaged and analyzed.* ***B:*** *The red line is the median cell length of E. coli BL21(DE3) pLysS expressing crGE; the black line is the average mCerulean3/mCitrine ratio of the same cells. The cell length was determined with the Feret's diameter in the PMT channel in ImageJ.* ***C:*** *The same as B with E. coli BL21(DE3) pLysS expressing crG18.*

300 mM NaCl, and the length returns to the value before the osmotic upshift after 0.5 h. After 60–90 minutes, the average cell length starts to increase as the cells resume growth. Afterwards, most of cells divide (apparent doubling time of 2 h), and accordingly the average cell length decreases. After this, the average length remains lower due to the adaptation of the cells to osmotic upshift. When we compare the cell length with the ratiometric FRET, we find that the crowding initially follows the cell volume; when the volume is low the crowding is high (shown in gray in Fig. 5B&C). After ~2 h, the crowding no longer follows the cell volume and both the volume and the ratiometric FRET decrease. Around ~2 h, the OD_{600} starts to increase again. Hence, the results indicate that the crowding is proportional to the cell volume immediately after the osmotic upshift, but that apparent correlation no longer holds at later times, that is, in the adaptation phase.

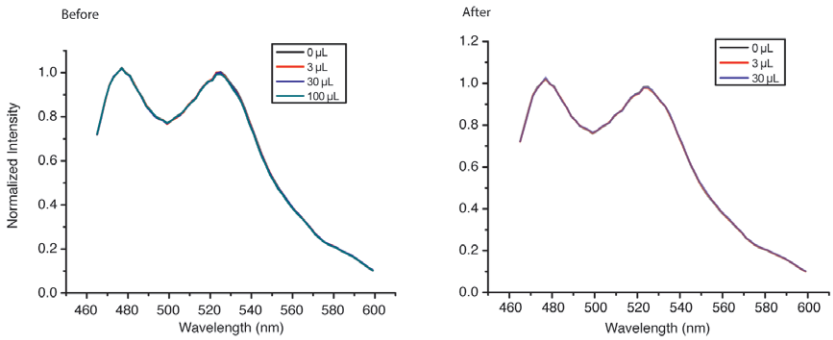

Fig. 6. Fluorescence spectra of crG18 sensor. *The crG18 was dissolved in 10 mM sodium phosphate (NaPi), 100 mM NaCl, pH 7.4 and titrated with different volumes of concentrated cell lysate. Left panel: titration with cell lysate before osmotic upshift; right panel: titration with cell lysate obtained 5 h after the osmotic upshift with 300 mM NaCl.*

Sensor performance during adaptation

The ratiometric FRET of the crowding sensor in living cells could be influenced by several factors, e.g. truncation/misfolding of the proteins, changes in refractive index and/or molecules binding to the sensor. To confirm that the ratiometric FRET reports genuine changes in excluded volume, rather than e.g. binding of specific molecules to the sensors, we investigated the influence of cell lysate on the sensor (**Fig. 6**). *E. coli* cells, grown for 5h in MOPS-glucose, with or without 300 mM NaCl, were lysed and the effect of cell lysate on purified crG18 sensor was tested. We did not find any effect of cell lysate. We only find a small effect of some metabolites (Proline, KCl, ATP, sucrose and aspartic acid) when tested at unphysiologically high concentrations.[25] For example, the ratiometric FRET decreased somewhat in the presence of 34 mM ATP, but the concentration in vivo is typically less than 10 mM[26]. Combined with previous work, in which we tested other relevant metabolites[18,19], we conclude that the changes in FRET signal are not likely due to small molecules binding to the sensors (Fig. 7).

To confirm that the sensor is not truncated during growth, we performed an SDS-PAGE analysis. The gels show that the sensors are not truncated in control and osmotically stressed cells (Fig. 8). To show that the ratiometric FRET signal is independent of the maturation of the fluorescent proteins, we excited mCitrine (FRET acceptor) in crGE directly at 488 nm, as well as mCerulean3 (FRET donor) at 405 nm. We determined the fluorescence intensity throughout the adaptation period (Fig. 9). The median intensity of mCerulean3 increased over the first 2h when the cells do not divide, while the fluorescence of mCitrine remains the same. The increase in intensity of mCerulean3, and not mCitrine, is likely due to increased maturation

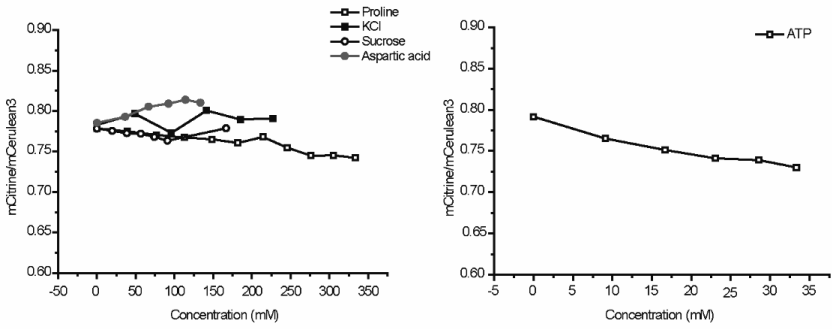

Fig. 7. The influence of small molecules on the ratiometric FRET of the crE6G2 sensor. *Experiments were done as described in the legend of Figure 7.*

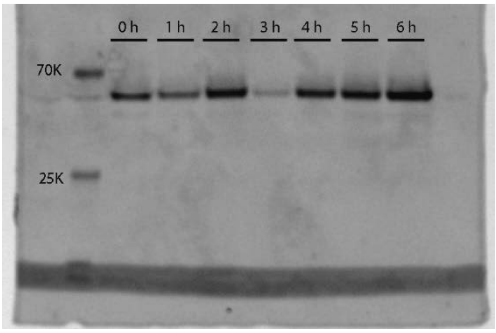

Fig. 8. In gel fluorescence of crGE sensor from E. coli. *The E. coli BL21(DE3) pLysS cells expressing crGE were incubated in MOPS medium at 30 °C and shaking at 200 rpm. The cells were shocked with 500 mM NaCl. The cells were lysed with Bugbuster 10X (Novagen®) and loaded onto a 12 % SDS-PAGE gel. The lower intensity of the 3h time point sample may have been caused by incomplete cell lysis.*

efficiency (see Chapter 4). After 2-3h, the relative concentration of fluorophores stays rather stable. Although improved maturation of mCerulean3 would also decrease the FRET, the gradual increase in maturation does not match the sharp decrease in FRET ratios that we see when cells start to grow. We thus conclude the reatiometic decrease not due to the truncation of sensor and the maturation of fluorescent protein.

Discussion

In this chapter, we determined the apparent crowding of *E. coli* during adaptation to high osmolality. We find that the crowding initially follows the cell volume but at later times in the adaptation phase the

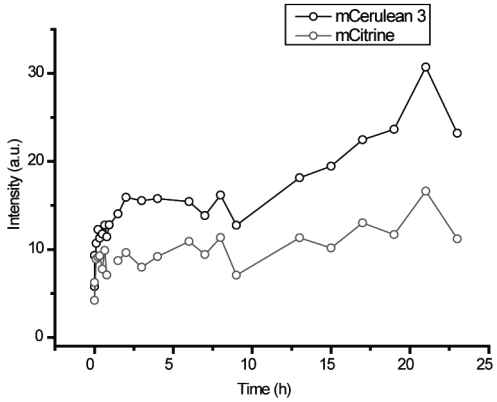

Fig. 9. The fluorescent intensity change of crGE in E. coli BL21(DE3) pLysS cells in MOPS medium. *The cells were treated with 300 mM NaCl upshift at time 0. Black circles are the median intensity of mCerulean3 in crGE, directly excited at 405 nm. Black circles are the median intensity of mCitrine, excited at 488 nm.*

parameters start to deviate. Remarkably, the apparent crowding stabilizes at a value below the one before the osmotic upshift. Our data bear resemblance to those of Gnutt et al.[27], who treated HeLa cells with 250 mM TMAO over a period of 16h. They also found a lower apparent crowding in the adaptation phase[28].

A decrease of crowding is typically explained by a lower volume fraction of macromolecules. However, Konopka et al.[17] determined the biopolymer fraction and the lateral diffusion of GFP in osmotically-shocked and adapted *E. coli* MC1655 grown in MOPS-glucose medium, and they noticed that there is not a simple relationship between biopolymer fraction and diffusion coefficient. The buoyant density of *E. coli* MC4100 grown in rich medium (TYG medium) increases with the osmolality of the medium[30]. The density of proteins is 1.2-1.4 g/cm^3 and higher than water (1.0 g/cm^3)[29], thus an increase indicates an increase of biopolymer fraction. Hence, the apparent crowding that we measure, and that by Gnutt et al., combined with the diffusion measurements by Konopka *et al.*, contrast with biopolymer volume fraction measurements.

Based on these observations, we hypothesize that the subcellular organization of the cytoplasm could change during adaptation to the osmotic upshift. The concentration of proteins and other macromolecules in the cytoplasm are typically close to their critical values[31,32] and the uneven distribution of hydrophilic, hydrophobic and charged surface areas of macromolecules enable the clustering of proteins and nucleic acid. As a result, cells may form subcellular organizations such as hyperstructures[33], intracellular bodies[34], and filaments[35]. The subcellular organizations can locally increase crowding

to an above-average level, leading to the formation of uncrowded areas elsewhere in the cytoplasm.

The subcellular organization is influenced by weak interactions, including electrostatic and hydrophobic interactions[36]. When cells adapt to the osmotic upshift, the weak interactions may change. As a result, the cells could form larger clusters and form less crowded regions in the cell, the effects of which would be altered by size and shape-based sorting of proteins by depletion forces. The crowding sensor may sense the less crowded regions and give a lower crowding value even though the total biomass volume fraction increases as the cell volume decreases.

Several other processes could contribute in forming larger hyper-structures and thus influence the crowding. During adaptation, DNA may increase its supercoiling[13,37], and simultaneously osmotic stress related genes[38] are expressed. The newly expressed proteins may have different surface properties, which changes the overall interactions e.g. hydrophobic interactions in the cell. Additionally, metabolites and compatible solutes may contribute to the subcellular organization of the cytoplasm. During adaption, the concentrations of ATP – which may act as a hydrotope[39] – may decrease. The decrease of ATP may result in formation of larger hyper-structures and decrease the crowding locally where the sensors locate.

Conclusions

In summary, we observe that the excluded volume changes as reported by our crowding sensors match with the volume changes upon osmotic upshift, but the correlation between volume and crowding does not hold in the adaptation phase. We hypothesize that biopolymer self-association creates a heterogeneous organization of the cytoplasm, resulting in regions with under- and overcrowding. The sensors might be biased towards probing the less crowded regions of the cell, hence the apparent decrease in macromolecular crowding.

References

1 Ellis, R. J. Macromolecular crowding: obvious but underappreciated. *Trends in Biochemical Sciences* **26**, 597-604, doi:10.1016/s0968-0004(01)01938-7 (2001).

2 Tan, C. M., Saurabh, S., Bruchez, M. P., Schwartz, R. & LeDuc, P. Molecular crowding shapes gene expression in synthetic cellular nanosystems. *Nature Nanotechnology* **8**, 602-608, doi:10.1038/nnano.2013.132 (2013).

3 Dix, J. A. & Verkman, A. S. Crowding effects on diffusion in solutions and cells. *Annual Review of Biophysics* **37**, 247-263, doi:10.1146/annurev.biophys.37.032807.125824 (2008).

4 Cayley, S. & Record, M. T. Large changes in cytoplasmic biopolymer concentration with osmolality indicate that macromolecular crowding may regulate protein-DNA interactions and growth rate in osmotically stressed Escherichia coli K-12. *Journal of Molecular Recognition* **17**, 488-496, doi:10.1002/jmr.695 (2004).

5 Nakano, S. & Sugimoto, N. Model studies of the effects of intracellular crowding on nucleic acid interactions. *Molecular Biosystems* **13**, 32-41, doi:10.1039/c6mb00654j (2017).

6 Samiotakis, A., Wittung-Stafshede, P. & Cheung, M. S. Folding, Stability and Shape of Proteins in Crowded Environments: Experimental and Computational Approaches. *International Journal of Molecular Sciences* **10**, 572-588, doi:10.3390/ijms10020572 (2009).

7 van den Berg, B., Ellis, R. J. & Dobson, C. M. Effects of macromolecular crowding on protein folding and aggregation. *Embo Journal* **18**, 6927-6933, doi:10.1093/emboj/18.24.6927 (1999).

8 Pilizota, T. & Shaevitz, J. W. Fast, Multiphase Volume Adaptation to Hyperosmotic Shock by Escherichia coli. *Plos One* **7**, doi:10.1371/journal.pone.0035205 (2012).

9 Chung, H. J., Bang, W. & Drake, M. A. Stress response of Escherichia coli. *Comprehensive Reviews in Food Science and Food Safety* **5**, 52-64, doi:10.1111/j.1541-4337.2006.00002.x (2006).

10 Wood, J. M. Bacterial responses to osmotic challenges. *Journal of General Physiology* **145**, 381-388, doi:10.1085/jgp.201411296 (2015).

11 Record, M. T., Courtenay, E. S., Cayley, D. S. & Guttman, H. J. Responses of E-coli to osmotic stress: Large changes in amounts of cytoplasmic solutes and water. *Trends in Biochemical Sciences* **23**, 143-148, doi:10.1016/s0968-0004(98)01196-7 (1998).

12 Shabala, L. et al. Ion transport and osmotic adjustment in Escherichia coli in response to ionic and non-ionic osmotica. *Environmental Microbiology* **11**, 137-148, doi:10.1111/j.1462-2920.2008.01748.x (2009).

13 Cheung, K. J., Badarinarayana, V., Selinger, D. W., Janse, D. & Church, G. M. A microarray-based antibiotic screen identifies a regulatory role for supercoiling in the osmotic stress response of Escherichia coli. *Genome Research* **13**, 206-215, doi:10.1101/gr.401003 (2003).

14 Bartholomaeus, A. et al. Bacteria differently regulate mRNA abundance to specifically respond to various stresses. *Philosophical Transactions of the Royal Society a-Mathematical Physical and Engineering Sciences* **374**, doi:10.1098/rsta.2015.0069 (2016).

15 Zhao, P. et al. Global transcriptional analysis of Escherichia coli expressing IrrE, a regulator from Deinococcus radiodurans, in response to NaCl shock. *Molecular Biosystems* **11**, 1165-1171, doi:10.1039/c5mb00080g (2015).

16 Metris, A., George, S. M., Mulholland, F., Carter, A. T. & Baranyi, J. Metabolic Shift of Escherichia coli under Salt Stress in the Presence of Glycine Betaine. *Applied and Environmental Microbiology* **80**, 4745-4756, doi:10.1128/aem.00599-14 (2014).

17 Konopka, M. C. et al. Cytoplasmic Protein Mobility in Osmotically Stressed Escherichia coli. *Journal of Bacteriology* **191**, 231-237, doi:10.1128/jb.00536-08 (2009).

18 Liu, B. Q. et al. Design and Properties of Genetically Encoded Probes for Sensing Macromolecular Crowding. *Biophysical Journal* **112**, 1929-1939, doi:10.1016/j.bpj.2017.04.004 (2017).

19 Boersma, A. J., Zuhorn, I. S. & Poolman, B. A sensor for quantification of macromolecular crowding in living cells. *Nature Methods* **12**, 227-+, doi:10.1038/nmeth.3257 (2015).

20 Neidhard.Fc, Bloch, P. L. & Smith, D. F. Culture medium for enterobacteria. *Journal of Bacteriology* **119**, 736-747 (1974).

21 Gebhardt, J. C. M. et al. Single-molecule imaging of transcription factor binding to DNA in live mammalian cells. *Nature Methods* **10**, 421-+, doi:10.1038/nmeth.2411 (2013).

22 van den Berg, J., Galbiati, H., Rasmussen, A., Miller, S. & Poolman, B. On the mobility, membrane location and functionality of mechanosensitive channels in Escherichia coli. *Scientific Reports* **6**, doi:10.1038/srep32709 (2016).

23 Kumar, N. & Kishore, N. Protein stabilization and counteraction of denaturing effect of urea by glycine betaine. *Biophysical Chemistry* **189**, 16-24, doi:10.1016/j.bpc.2014.03.001 (2014).

24 Perroud, B. & Lerudulier, D. Glycine betaine transport in Escherichia coli: osmotic modulation. *Journal of Bacteriology* **161**, 393-401 (1985).

25 Bennett, B. D. et al. Absolute metabolite concentrations and implied enzyme active site occupancy in Escherichia coli. *Nature Chemical Biology* **5**, 593-599, doi:10.1038/nchembio.186 (2009).

26 Yaginuma, H. et al. Diversity in ATP concentrations in a single bacterial cell population revealed by quantitative single-cell imaging. *Scientific Reports* **4**, doi:10.1038/srep06522 (2014).

27 Gnutt, D., Gao, M., Brylski, O., Heyden, M. & Ebbinghaus, S. Excluded-Volume Effects in Living Cells. *Angewandte Chemie-International Edition* **54**, 2548-2551, doi:10.1002/anie.201409847 (2015).

28 Gnutt, D., Brylski, O., Edengeiser, E., Havenith, M. & Ebbinghaus, S. Imperfect crowding adaptation of mammalian cells towards osmotic stress and its modulation by osmolytes. *Molecular bioSystems*, doi:10.1039/c7mb00432j (2017).

29 Milo, R. & Phillips, R. Cell Biology by the Numbers. (2015).

30 Baldwin, W. W., Sheu, M. J. T., Bankston, P. W. & Woldringh, C. L. Changes in buoyant density and cell size of Escherichia coli in response to osmotic shocks. *Journal of Bacteriology* **170**, 452-455 (1988).

31 Tartaglia, G. G., Pechmann, S., Dobson, C. M. & Vendruscolo, M. Life on the edge: a link between gene expression levels and aggregation rates of human proteins. *Trends in Biochemical Sciences* **32**, 204-206, doi:10.1016/j.tibs.2007.03.005 (2007).

32 Schavemaker, P. E., Śmigiel, W. M. & Poolman, B. Ribosome surface properties may impose limits on the nature of the cytoplasmic proteome. *Elife*, doi:10.7554/eLife.30084 (2017).

33 Norris, V. et al. Functional taxonomy of bacterial hyperstructures. *Microbiology and Molecular Biology Reviews* **71**, 230-253, doi:10.1128/mmbr.00035-06 (2007).

34 O'Connell, J. D., Zhao, A., Ellington, A. D. & Marcotte, E. M. Dynamic Reorganization of Metabolic Enzymes into Intracellular Bodies. *Annual Review of Cell and Developmental Biology*, **28**, 89-111, doi:10.1146/annurev-cellbio-101011-155841 (2012).

35 Petrovska, I. et al. Filament formation by metabolic enzymes is a specific adaptation to an advanced state of cellular starvation. *Elife* **3**, doi:10.7554/eLife.02409 (2014).

36 Cohen, R. D., Guseman, A. J. & Pielak, G. J. Intracellular pH modulates quinary structure. *Protein Science* **24**, 1748-1755, doi:10.1002/pro.2765 (2015).

37 Higgins, C. F. et al. A physiological role for DNA supercoiling in the osmotic regulation of gene expression in S. typhimurium and E. coli. *Cell* **52**, 569-584, doi:10.1016/0092-8674(88)90470-9 (1988).

38 Wood, J. M. et al. Osmosensing and osmoregulatory compatible solute accumulation by bacteria. *Comparative Biochemistry and Physiology a-Molecular and Integrative Physiology* **130**, 437-460, doi:10.1016/s1095-6433(01)00442-1 (2001).

39 Patel, A. et al. ATP as a biological hydrotrope. *Science* **356**, 753-756, doi:10.1126/science.aaf6846 (2017).